Nuclear Engineering and Design 238 (2008) 3136–3144

Contents lists available at ScienceDirect

Nuclear Engineering and Design

journal homepage: www.elsevier.com/locate/nucengdes

Design and optimization of a multistage turbine for helium cooled reactor

R.A. Van den Braembussche [a,*], J.F. Brouckaert [a], G. Paniagua [a], L. Briottet [b]

[a] *von Karman Institute for Fluid Dynamics, Sint-Genesius-Rode, Belgium*
[b] *Commissariat à l'Energie Atomique, Grenoble, France*

ARTICLE INFO

Article history:
Received 6 April 2007
Received in revised form 14 January 2008
Accepted 14 January 2008

ABSTRACT

This paper describes the aerodynamic design and explores the performance limits of a 600 MWt multistage helium turbine for a high temperature nuclear reactor closed cycle gas turbine. The design aims for maximum performance while limiting the number of stages for reasons of rotor dynamics and weight.

A first part discusses the arguments that allow a preliminary selection of the overall dimensions by means of performance prediction correlations and simplified stress considerations. The rotational speed being fixed at 3000 rpm, the only degrees of freedom for the design are: the impeller diameter, number of stages and stage loading.

The optimum load distribution of the different stages, the main flow parameters and the blade overall dimensions are defined by means of a 2D through-flow analysis method. The resulting absolute and relative flow angles and span-wise velocity variation are the input for a first detailed design by an inverse method. The latter defines the different 2D blade sections corresponding to prescribed optimum velocity distributions.

The final 3D blade definition is made by means of a computer based 3D-DESIGN system developed at the von Karman Institute. This method combines a 3D Navier–Stokes (NS) solver, Database, Artificial Neural Network and Genetic Algorithm into a two level optimization technique for compressor and turbine stages. The use of 3D Navier–Stokes solvers allows full accounting of the secondary flow losses and optimization of the compound leaning of the stator vanes.

The performance of the individual stages is used to define the multistage operating curves. The last part of the paper describes an evaluation of the cooling requirements of the first turbine rotor.

1. Introduction

The use of a helium gas turbine power conversion system in the primary cooling circuit of nuclear reactors has several advantages (Bammert et al., 1969). The high energy density of the working fluid results in a compact conversion system. The isentropic exponent of helium (∼1.667) is much larger than for air (∼1.4) and allows a higher thermal cycle efficiency. The high speed of sound of helium (∼2000 m/s at turbine inlet) results in very low Mach number flows. This simplifies the design procedure because it allows the use of well-proven design systems and facilitates the scaling of existing components to different operating conditions.

However, the geometry of helium turbomachines differs from the one of gas turbines operating in air because of the nature of the working fluid. Theory shows that the same isentropic exponent is a prerequisite for similarity (Roberts and Sjolander, 2005). Turbomachinery characteristics, even properly non-dimensionalized, will vary if the γ of the working fluid varies. Hence existing high performance turbomachinery components, developed for air, cannot be recuperated for helium applications. The design of completely new turbomachinery components is required.

The main difference between helium and air turbines is the much larger change in blade height of the latter one. The meridional contour of highly loaded air turbines is strongly diverging whereas helium turbines have an almost constant blade height, allowing the use of nearly identical stages from inlet to outlet. This means that the design of a helium turbine can be concentrated on one stage.

Smaller helium turbines have been developed and tested in the past (Bammert et al., 1974). Larger units are currently being investigated (Ballot, 2002; McDonald et al., 1975; Muto et al., 1999). The present paper describes the different steps that have been taken in the design and optimization of a large multistage helium turbine. The purpose is to get an idea of the overall dimensions and the achievable performance.

A first layout, based on overall performance and stress considerations, is followed by a more refined definition of the meridional contour and local flow angles. A first definition of the blade sections by means of an inverse method is followed by the 3D analysis

* Corresponding author.
E-mail addresses: vdb@vki.ac.be (R.A. Van den Braembussche), brouckaert@vki.ac.be (J.F. Brouckaert), paniagua@vki.ac.be (G. Paniagua), briottet@chartreuse.cea.fr (L. Briottet).

0029-5493/$ – see front matter © 2008 R.A. Van den Braembussche. Published by Elsevier B.V. All rights reserved.
doi:10.1016/j.nucengdes.2008.01.024

Nomenclature

c	blade chord (m)
D_H	hydraulic diameter (m)
h	blade height (m) or heat transfer coefficient (W/m^2/K)
H	total enthalpy (J/kg)
k	heat conductivity of the fluid (W/m/K)
L	length (m)
m	mass flow (kg/s)
N	number of stages
P	pressure (Pa)
r	radius (m) or degree of reaction
s	blade contour length (m)
T	temperature (K)
U	peripheral velocity (m/s)
V	absolute velocity (m/s)

Greek symbols

Φ	flow coefficient
α	absolute flow angle (°) measured form axial
β	relative flow angle (°) measured from axial
η	efficiency
λ	lean angle (°)
ν	kinematic viscosity (m^2/s) or Young's modulus
θ	turning (°)
ρ	density (kg/m^3)
σ	stresses (MPa)
ω	rotational speed (rad/s)
Ψ	load coefficient

Subscripts

ax	axial component
h	of helium
m	of the metal
TS	total to static
TT	total to total

and a manual improvement of a typical stage by means of a 3D Navier–Stokes (NS) solver. The final design step is an evaluation of the possible performance improvements by means of bowed stator vanes. The last part of the paper describes the prediction of the performance of the multistage turbine and an evaluation of the cooling requirements of the first turbine rotor.

2. Design considerations

The operating conditions for the turbine are listed in Table 1. Before carrying out a detailed aerodynamic design one must fix the overall geometrical parameters such as: number of stages, loading per stage, overall dimensions of the turbine and targeted efficiency.

The Smith diagram (Fig. 1) relates the stage load coefficient $\Psi = \Delta H/U^2$ and flow coefficient $\Phi = V_{ax}/U$ to the efficiency (Smith, 1965). The curves are obtained for different families of gas turbine stages at zero tip leakage and do not account for mechanical losses. One observes that the stage efficiency depends on the combination of the load and flow coefficient.

Table 1
Design conditions for the turbine

Working gas	Helium
Rotational speed	3000 rpm
Mass flow rate	316 kg/s
Inlet temperature	1121.2 K
Outlet temperature	783.2 K
Inlet pressure	70.1 bar
Outlet pressure	26.4 bar
Pressure ratio	2.65

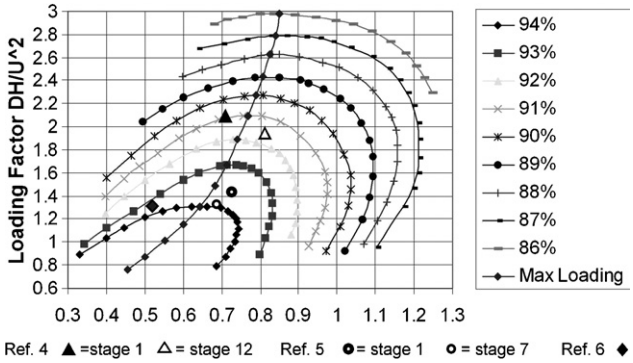

Fig. 1. Turbine stage efficiency at zero tip leakage in function of load and flow coefficient. Symbols refer to similar helium turbine designs (Ref. 4: Ballot, 2002, Ref. 5: McDonald et al., 1975, Ref. 6: Muto et al., 1999).

The present parametric study has been carried out for the operating points along the parabolic line crossing the lines of constant efficiency in the Smith diagram. Each point on this line corresponds to a couple (Ψ_{max}, Φ) and, in what follows, is referenced by the corresponding efficiency. Designing for these load values will result in the smallest possible number of stages for the required work output at the targeted efficiency. Symbols on that graph correspond to other large helium turbine designs described in the corresponding reference. Their operating point is also close to that maximum load line.

At a given load coefficient Ψ the required work output ΔH_{total} can be obtained with different number of stages or peripheral speeds.

$$\Psi = \frac{\Delta H_{stage}}{U^2} = \frac{\Delta H_{total}}{N_{stages}} \frac{1}{U^2} \tag{1}$$

Substituting in (1) the Ψ_{max} values corresponding to the maximum loading line, defines for each efficiency the minimum number of stages as a function of peripheral speed (Fig. 2). Lower Ψ values allow higher efficiencies but require an increase of peripheral velocity or more stages at given peripheral velocity. Larger Ψ values result in a smaller number of stages but also in a lower efficiency.

The targeted efficiency fixes the number of stages that is required. If the design is constrained by a maximum number of stages, the achievable efficiency for the required work output will be limited by the maximum peripheral speed U. At the prescribed rotational speed (3000 rpm), this limit defines the radius of the turbine disk, as shown in Fig. 3.

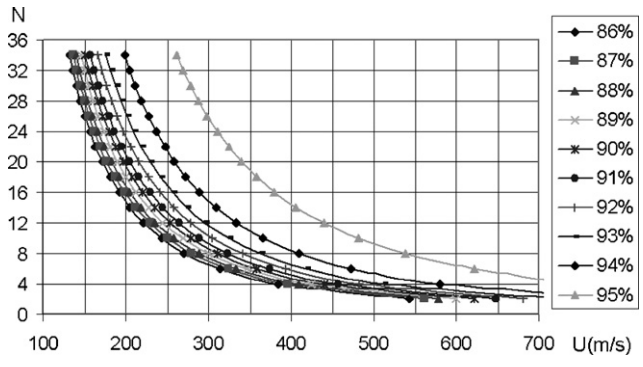

Fig. 2. Number of stages vs. peripheral speed for different efficiencies.

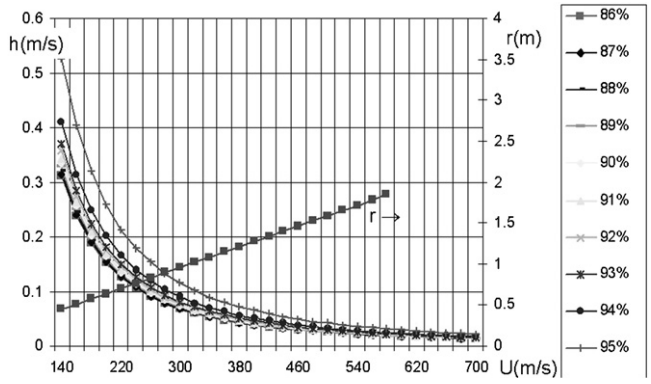

Fig. 3. Blade height and mean radius as a function of peripheral speed at 3000 rpm.

The flow coefficient Φ fixes the axial (through flow) velocity and at given radius also the blade height h.

$$h = \frac{m}{2\pi r \rho \Phi U} \tag{2}$$

Substituting the flow coefficient Φ, corresponding to the "maximum loading" line, defines the optimum blade height h for each value of the efficiency and peripheral speed (Fig. 3).

At given mass flow, the blade height h is inversely proportional the flow coefficient and the square of the peripheral speed. Increasing U leads to smaller blade heights and the secondary flows, generated by the cross flows on the annular walls, occupy a larger portion of the flow passage. This is not recommended from an aerodynamic point of view because it causes an increase of the secondary flow losses (Sieverding, 1985a). The corresponding drop in efficiency for present application can be estimated at less than 1% points at $U = 300$ m/s to 4% points at $U = 500$ m/s (Fig. 4).

The smaller axial velocity, resulting from smaller Φ values, not only leads to longer blades but, at given Ψ value, also to larger flow angles (more tangential flow). The latter ones limit the favorable effect of an increased blade length on the secondary flow. Longer blades also cause higher stresses at the blade root. Hence, a careful balance between the various parameters, playing an important role into the aerodynamic and mechanical design of the machine, is required.

Smaller blade heights cause lower stresses at the blade root but, at constant Φ, require larger peripheral speeds and increase the stresses in the rotor disk. The latter are defined by:

$$\sigma_{\max} = \frac{3+\nu}{4}\rho_m \omega^2 r_{\max}^2 \left(1 + \frac{1-\nu}{3+\nu}\frac{r_{\max}^2}{r_{\min}^2}\right) \tag{3}$$

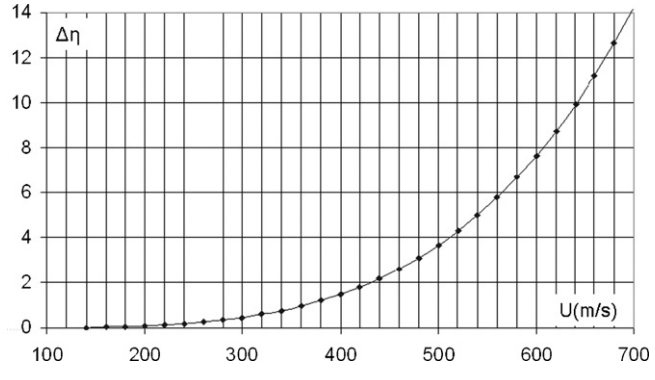

Fig. 4. Variation of efficiency due to secondary flow losses as a function of peripheral speed at 3000 rpm.

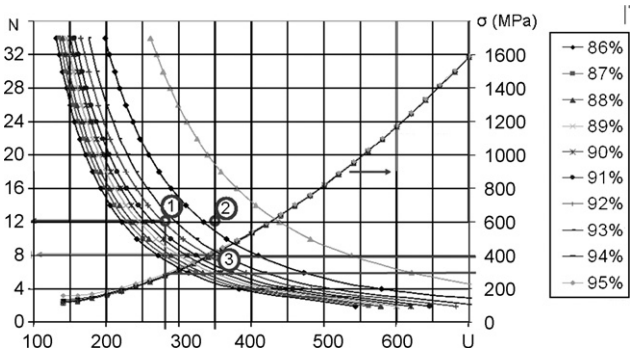

Fig. 5. Number of stages and stress in the turbine disk vs. peripheral speed.

where $r_{\max}$ and $r_{\min}$ are the outer and inner diameter of the rotor disk. The stresses shown in Fig. 5 are for an In718 rotor with an outer radius of 0.8 m and a radius ratio $r_{\max}/r_{\min} = 0.7$.

The maximum allowable stress level is function of the metal temperature and has an important impact on the expected lifetime of the equipment (creep). One has to make a compromise between the mechanical constraints and the aerodynamic performance requirements. Fig. 5 considers both by overlaying the variation of the rotor disk stresses into Fig. 2. Several choices may be of interest.

Limiting the number of turbine stages to 12 and the peripheral velocity to 280 m/s (point Nr. 1) allows an efficiency of 92% and results in a maximum mechanical stresses of 300 MPa. Increasing the tip speed to 350 m/s, while keeping 12 stages, could lead to a gain of more than 2% in efficiency (point Nr. 2) but at the cost of an increase in maximum stress level to 400 MPa. At this stress level one could also reduce the number of stages to 8 and obtain the same efficiency as for the 12-stage configuration (point Nr. 3).

It has been decided to investigate further the design point Nr. 1 because it is on the safe side in terms of stresses and rotor-dynamics and has an acceptable efficiency.

3. Quasi 3D turbine design

A first optimization of the detailed turbine geometry (variation of blade height and flow angles) is made by means of the VKI Meanline Analysis Program (MAP) (De Michele et al., 1975). This performance prediction method is based on the equations of radial equilibrium and makes use of the different turbine correlations for profile, secondary flow, clearance and gap losses to predict the turbine performance. The results presented here are obtained with the correlations of Soderberg (Sieverding, 1985b). The program predicts the flow variation from hub to shroud at all sections between the stators and rotors and estimates the performance (work output and efficiency). Applying this program to different geometries allows defining the optimum combination of flow angles and blade height over the different turbine stages.

The proposed 12 stage turbine has a load factor Ψ of 2.07 for all intermediate stages. A slightly higher ($\Psi = 2.19$) value is required for the first stage, because of the axial inflow. A lower value ($\Psi = 1.69$) at the last stage results in an axial outflow and minimizes the kinetic energy losses in the ducts.

The optimized flow parameters for stages 1, 2, 11 and 12 are listed in Table 2. They are almost identical from stage 1 to 11 with a degree of reaction $r = 0.3$. The last stage operates with a lower degree of reaction ($r = 0.19$) to obtain a nearly axial outlet flow. The program predicts a shaft power (neglecting the mechanical losses and inlet/outlet duct losses) of 569.58 MW, an overall total-to-total and total-to-static efficiency of, respectively, $\eta_{TT} = 93.38\%$

Table 2
Turbine lay-out

	Stage 1	Stage2	Stage 11	Stage 12
Stator				
$\alpha_{1stator}$ [°]	0.0	−30.29	−24.37	−23.49
$\alpha_{2stator}$ [°]	68.98	69.00	65.89	64.28
θ_{stator} [°]	68.98	99.29	90.26	87.77
$Ma_{abs,\ stator}$ [−]	0.260	0.264	0.309	0.304
Pitch/chord [−]	1.051	1.068	1.062	1.054
$N_{blades,\ stator}$	51	60	65	67
Rotor				
β_{1rotor} [°]	49.20	49.22	43.58	39.48
β_{2rotor} [°]	−63.95	−63.77	−59.91	−52.39
θ_{rotor} [°]	113.1	113.0	103.5	91.87
$Ma_{rel,\ rotor}$ [−]	0.21	0.213	0.252	0.214
Pitch/chord [−]	1.264	1.265	1.264	1.267
$N_{blades,\ rotor}$	137	138	144	151
Stage				
η_{TT}	0.9256	0.9144	0.9248	0.9284

and η_{TS} = 92.32%. These values are in agreement with the predictions based on the Smith correlation.

This program also provides the flow angles at inlet and outlet of each rotor and stator (Fig. 6), required for a detailed blade design by means of the inverse design method INVC (Van den Braembussche et al., 1989; Leonard, 1992). The latter starts with the analysis of a first guess of the blade geometry by means of a potential flow solver. The difference between the calculated and required velocity is used as an input for the modification algorithm based on a transpiration technique. This provides a new blade shape on which the velocity distribution is now closer to the desired one. The updating of the blade shape is repeated until the calculated velocity distribution matches the required one. A major advantage of this method is its very short design cycle and easy off-design analysis since the same code is used for the blade design and for the analysis at different inlet conditions. Its main drawback is its limitation to 2D potential flows.

The velocity distribution shown in Fig. 7 is the one imposed at the stator mid-span section. It is considered as optimal because it shows a continuous flow acceleration along the whole pressure side and up to 50% of the suction side after which it is followed by a moderate deceleration towards the trailing edge. Similar distributions are imposed at hub, mean and tip section of both stator and rotor and should guarantee a good performance of the turbine.

The 3D blades are obtained by stacking the centroids of the 2D blade sections along a radius. The layout of the first two stages is schematically shown in Fig. 8. The blade shape of stage 2 is repeated in all the following stages. The lower number of stator blades results in a longer chord length to obtain the selected pitch/chord ratio. Only the blade height and blade number are

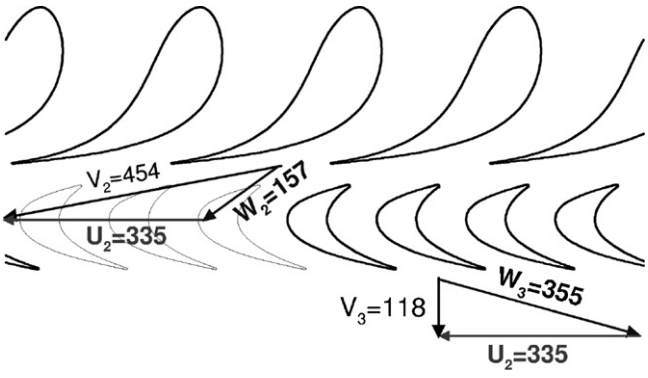

Fig. 6. Velocity triangles in the last stage.

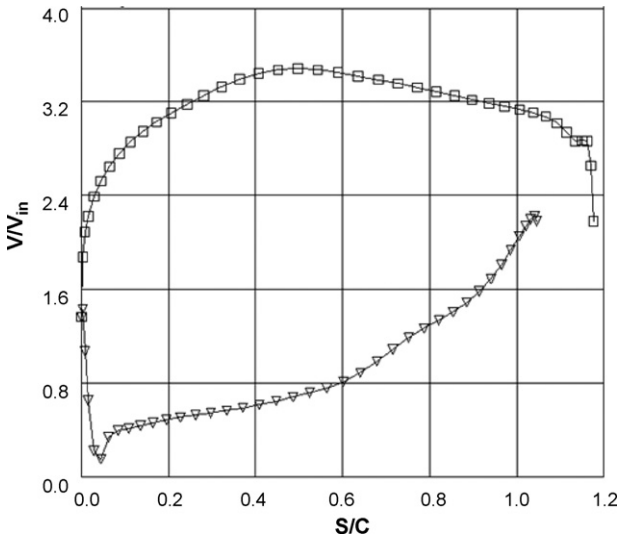

Fig. 7. Imposed velocity distribution at stator mid-section.

adjusted at each stage to maintain the same Φ value and pitch to chord ratio throughout the whole turbine. The hub radius is kept constant and the shroud radius increases slowly to compensate for the decreasing density between inlet to outlet. The increase of the shroud radius is much smaller than for air turbines and justifies the assumption that all stages have an identical blade shape and performance. Hence further optimization can be limited to only one stage.

4. 3D turbine design

The final geometry has been selected after analyzing several 3D geometries by means of the multistage Navier–Stokes solver TRAFMS (Arnone, 1994). This program predicts the 3D viscous flow in compressor and turbine stages, with and without tip clearance. The Reynolds-averaged Navier–Stokes equations are solved using a Runge–Kutta scheme in conjunction with accelerating techniques such as: local time stepping, residual smoothing and Full-Approximation-Storage (FAS) multigrid. The equations are discretized using finite volumes and a cell-centered scheme with 2nd and 4th order artificial dissipation. Eigenvalue scaling assures a very low level of artificial viscosity. The blade to blade grid generation process is based on an elliptic procedure that solves the discretized Poisson equations using a point relaxation scheme. The three

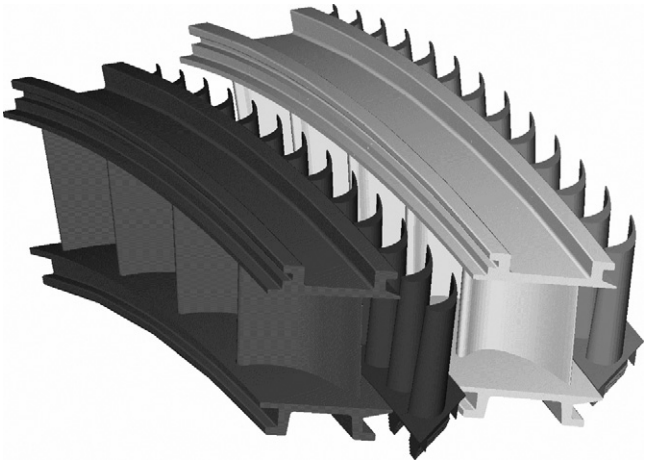

Fig. 8. Initial layout of first two stages.

dimensional grid is generated by stacking the two dimensional non-periodic grids. 400 000 grid cells are used in, respectively, the stator and rotor.

The two-layer mixing length model of Baldwin and Lomax is used to compute the turbulent quantities. Turbulent flows are assumed on all blade- and end walls because of the uncertainty about the influence of free stream turbulence on transition in multistage machines. This is on the safe side because it can be expected that in spite of the free stream turbulence in multistage turbines, the large accelerating flow zones on pressure and suction side will locally result in laminar boundary layers and hence lower losses.

The multistage program TRAFMS uses circumferential averaging at the interface between stationary and rotating rows. Care has been taken to avoid that this averaging could influence the solution by imposing circumferentially uniform flow too close to the leading edge. The multistage environment is simulated by imposing spanwise non-uniform flow conditions at the inlet of the numerical domain of each stage. They are obtained by superposing the flow angle and total pressure distortion at the exit of the stage on the average values at the inlet.

4.1. Stator blade section redesign

Stage 2 has been selected for further 3D optimization. It already has non-uniform inlet flow and the smallest blade height, hence highest secondary flow losses. The mid-span average inlet conditions are the ones listed in Table 2.

Although the 2D calculations of the stator and rotor blade sections showed very good Mach number distributions and low losses, the first 3D calculations indicated efficiencies below the ones predicted by the through flow analysis program. This lack of performance was attributed to the large secondary losses, generated in the highly loaded stages ($\Psi > 2$) that could not be predicted by the potential 2D inverse design.

The secondary flows (Fig. 9) result from the migration of the hub and shroud wall boundary layer from the blade pressure side towards the suction side. The consequence is a vortical flow and an accumulation of losses in the hub and shroud suction side corner. The stator iso-Mach surfaces at mid-section and hub are shown in, respectively, Fig. 10(a and b). A near optimum flow path is observed at mid-section. The streamline pattern on the stator hub wall indicates a saddle point quite upstream of the leading edge and return flow along the pressure side. This is a consequence of the pressure

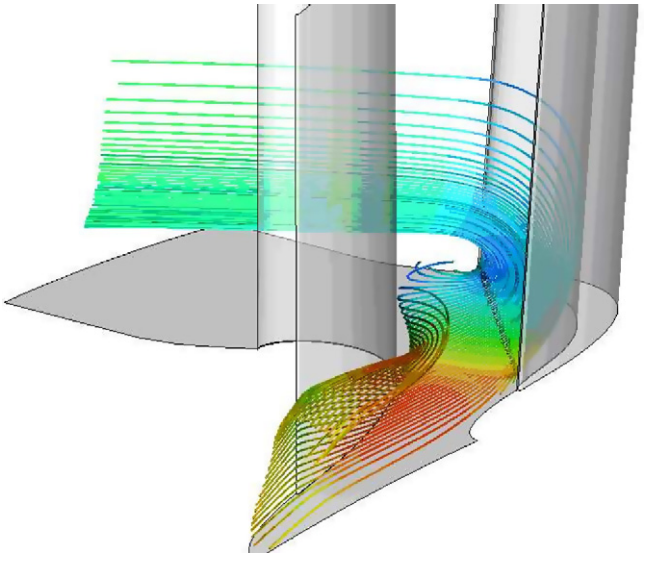

Fig. 9. Secondary flow pattern near hub.

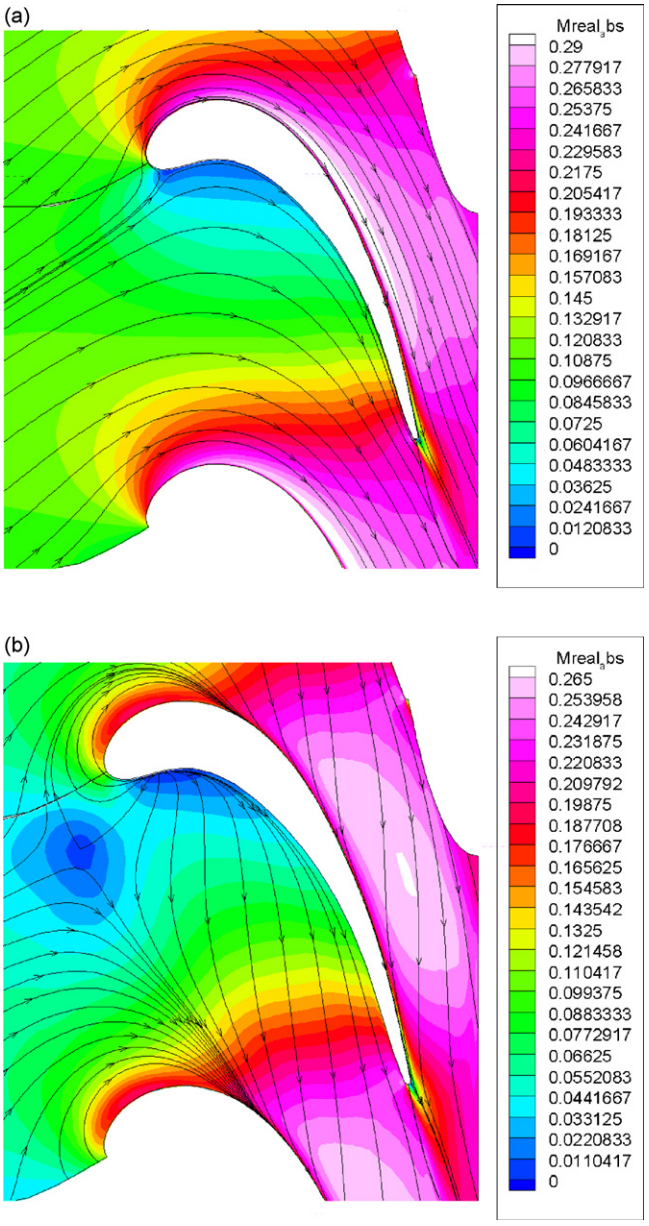

Fig. 10. (a) Iso-Mach surface and streamline pattern at the stator mid-section. (b) Iso-Mach surface and streamline pattern at the stator hub wall.

increase along the first part of the pressure side for the near wall inlet flow conditions.

An optimum blade for 2D flows is not necessarily optimal for 3D flow. Several modifications of the original blades have been made and verified in an attempt to increase the efficiency. The most important ones are (Fig. 11):

- A redesign of the blade leading edge to create an accelerating flow along the pressure side.
- An increase of the stator blade number from 58 to 77 and a reduction of the blade chord to keep the pitch to chord ratio constant. This results in a 25% increase of the aspect ratio and reduces the impact of secondary losses on the overall performance.

The analysis of the new stage shows an increase in stage efficiency by 1% point and a corresponding increase in power output. The favorable effect of these modifications is obvious when comparing the stator, rotor and stage span-wise distribution of efficiency

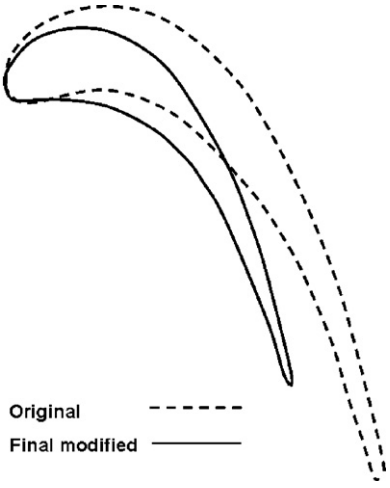

Fig. 11. Original vs. redesigned stator blade.

of the original stage (Fig. 12) with the one of the redesigned stage (Fig. 13). The shape of the efficiency curves is globally the same but the curves of the new stator have a higher value. One observes that the low efficiency problems at the stator non-dimensional blade heights of 0.1 and 0.9 have been considerably reduced. Also the stator mid-span total-to-static efficiency has increased by 2.5% from an approximate 92.5% to a little over 95%, and the stage total-to-total efficiency, at the same radius, has increased by 4.5% from 88% to 92.5%.

The performance of the new turbine stage has also been verified by means of the NUMECA and ANSYS commercial solvers. Both confirm the results of the TRAFMS calculations within the uncertainty margin. Calculations with ANSYS show a possible increase of efficiency by 0.7% point when using the real gas characteristics of helium.

5. Full 3D stator blade optimization

A second way to minimize the secondary flow losses is by introducing compound lean, i.e. by bending the blades in the circumferential direction. The consequence is a span-wise variation

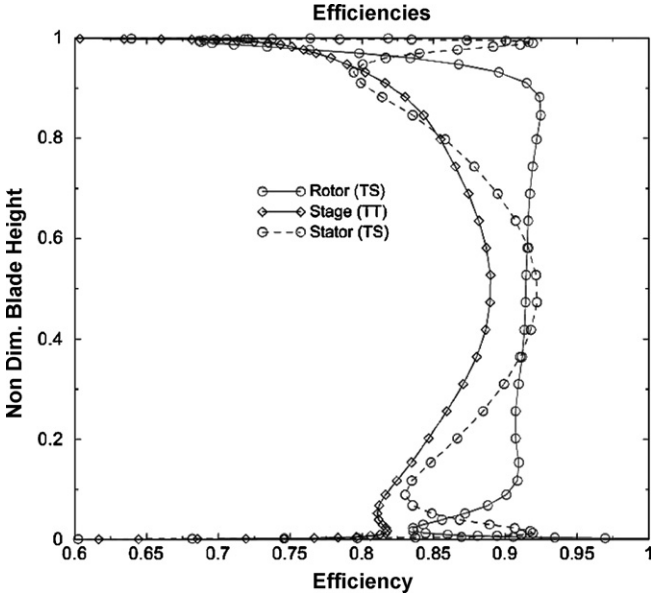

Fig. 12. Span-wise variation of the second stage efficiencies (original design).

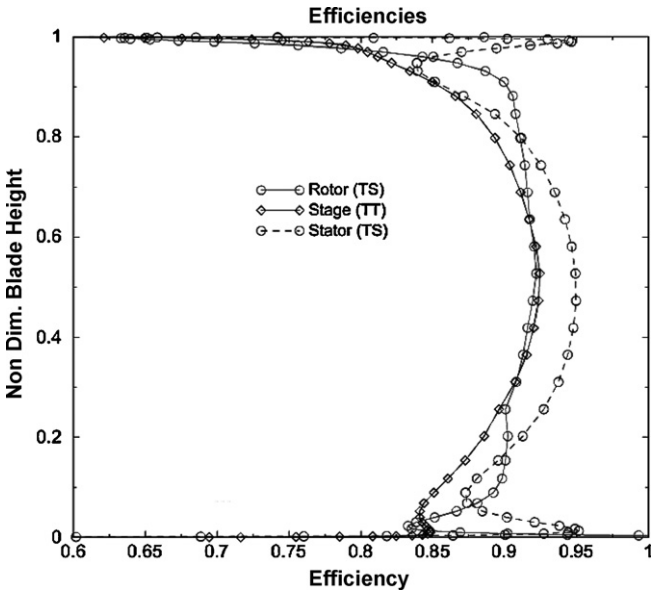

Fig. 13. Span-wise variation of the second stage efficiencies (new design).

of the static pressure, resulting in an increased blade loading at mid-section, a decreased loading near the end walls and a redistribution of the secondary flow over the blade height. The problem is to find the optimum bending such that this redistribution results in a reduction of the overall losses. This full 3D optimization is limited to the stators because centrifugal forces could create unacceptable stresses and deformations when leaning the blades of the rotating components. All flow analyses are made with the stator in front of the rotor in order to fully account for the impact of the change in stator outflow on rotor performance.

5.1. Optimization method

This redesign is achieved by means of the 3D optimization program developed at the von Karman Institute (Pierret and Van den Braembussche, 1999a,b). The main characteristic of the method is the use of a surrogate model of the original complicated analysis method (the 3D Navier–Stokes solver) to speed up the convergence (Fig. 14). The model consists of an Artificial Neural Network (ANN) trained on a DATABASE. The performance evaluations by the ANN are very fast and the larger number of evaluations required by the GENETIC ALGORITHM for the optimization is no longer a critical issue. At the end of this optimization phase, one has recourse to the high-fidelity Navier–Stokes solver TRAFMS to verify the lower-fidelity ANN predictions. The PERFORMANCE predicted by the Navier–Stokes solver and the corresponding geometry are added to the DATABASE and a new optimization cycle is started. It is expected that after a new LEARNING on an extended DATABASE the PREDICTION by this ANN will be more accurate.

The optimization cycle is stopped once the ANN predicted PERFORMANCE agrees with the Navier–Stokes one, i.e. when the optimization has been made with an analysis system that is as accurate as the Navier–Stokes solver. This system allows a much faster optimization of turbomachinery components than a classical gradient or Genetic Algorithm method because the number of Navier–Stokes solutions is drastically reduced.

5.2. Parameterized geometry and database

A critical element in the success of an optimization method is its capacity to generate a large variety of different but physically

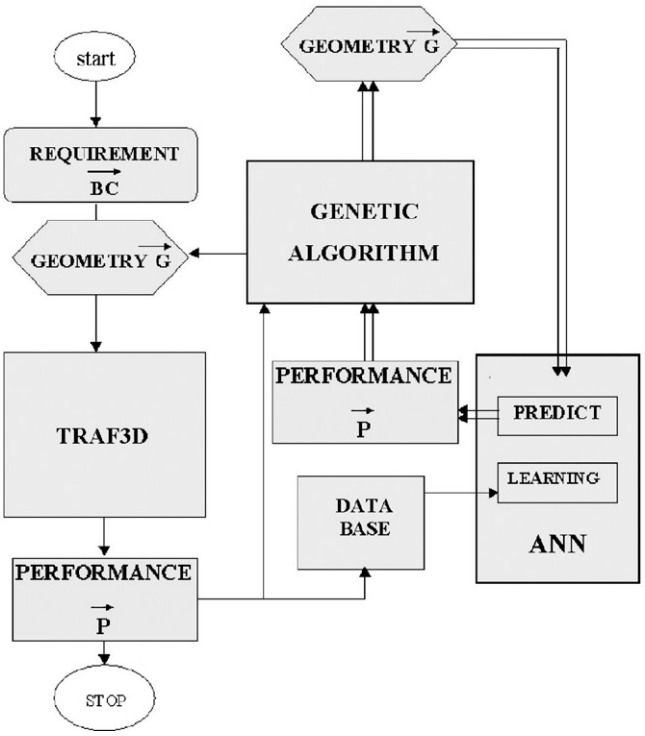

Fig. 14. Flowchart of von Karman Institute turbomachinery optimization system.

realistic shapes by means of a minimum number of parameters. A parametric definition of the blade geometry is therefore required. The full 3D blade definition places the optimized 2D blade sections along a stacking line defined by 7 parameters (Fig. 15). The design space is restricted to feasible geometries by limiting these 7 parameters to the values listed in Table 3.

A DOE (Design of Experiment) technique is used to define the 17 geometries stored in the initial DATABASE. This favors an optimum spreading of the Database samples over the whole design space and increases the accuracy of ANN predictions. A few typical geometries are shown in Fig. 16 to illustrate the large variety of geometries that have been generated and analyzed.

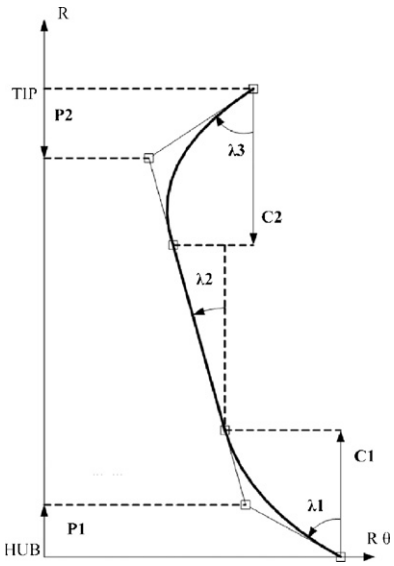

Fig. 15. Definition of the parameterized stacking line.

Table 3
Limits of design parameters

	Lower limit	Upper limit
λ_1 (°)	0	20
λ_2 (°)	−15	15
λ_3 (°)	−20	0
C_1 (% h)	0	50
C_2 (% h)	0	50
P_1 (% C_1)	0	99
P_2 (% C_1)	0	99

5.3. Results of 3D optimization

The results of the Navier–Stokes analysis of all the DATABASE samples show very little variation. The influence of geometrical modifications on the performance is of the same order as the uncertainty of the Navier–Stokes solver. The 3D optimization did not lead to a measurable improvement of the performance. Even after 19 optimization cycles the optimiser could not find a geometry that was significantly better than the initial prismatic one. This is somewhat surprising since the same approach resulted in a 0.3% point improvement in overall efficiency when applied to the initial stator blade.

The large aspect ratio of the stator blades and hence the small secondary flow losses are likely to be at the origin of this. Another explanation is that bending the blades results in a redistribution of the secondary flows over the blade height but does not necessarily decrease the losses. Only a marginal increase in efficiency is experienced when starting the optimization from a prismatic blade with optimized 2D blade sections. Most spectacular improvements by compound lean, reported in the literature, have been achieved when starting from blades with low initial performance, suggesting that there was a problem that could be alleviated by bending the blades (Yershov et al., 2007).

In conclusion, it turns out that the complication of leaning the stator blades does not contribute to a significant performance improvement and that it is of no use in present design. The achieved performance is in agreement with the one predicted by the Smith correlation taking into account that the correlation does not account for clearance losses.

6. Multistage and off-design performance

The multistage geometry is defined in function of the single stage performance by imposing that the design flow coefficient Φ, efficiency η and load coefficient Ψ are the same at every stage from inlet to outlet. The corresponding stage enthalpy rise and efficiency (Eq. (4)) allow defining the stage outlet temperature and pressure in function of the inlet flow conditions.

$$\eta = \frac{\Psi \cdot U^2}{C_p((P_{in}/P_{out})^{\gamma-1/\gamma} - 1)} \tag{4}$$

Hence the outlet density can be calculated and the next stage blade height is obtained by satisfying the continuity in function of the local axial velocity corresponding to the design flow coefficient Φ (Eq. (2)). Hence the only difference between the individual stages is the blade length.

The single stage off-design performance is obtained by analyzing the optimized turbine stage at different pressure ratios. This induces a change in mass flow and hence of the turbine exit flow conditions that are the next stage inlet conditions. Because all stages are similar, they also define the present stage inlet conditions. An iterative procedure is started whereby these inlet conditions are updated until the inlet flow angle distribution agrees with the outlet one. The result is the stage load coefficient and effi-

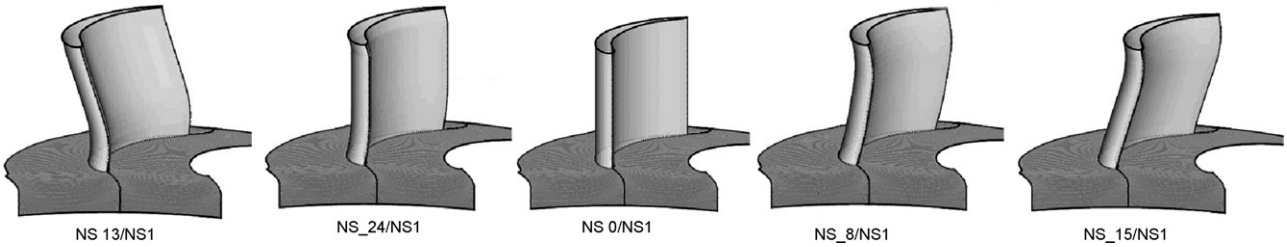

Fig. 16. Selection of some typical 3D stator geometries.

ciency for different flow coefficients between minimum pressure drop and choking mass flow.

Following procedure allows the calculation of the complete multistage performance in function of the single stage non-dimensional off-design performance. The axial velocity at a given off-design mass flow and hence the flow coefficient Φ can be calculated from the continuity equation as a function of the local blade height and local inlet flow conditions (pressure, temperature and density). The off-design performance curve provides the corresponding Ψ value and efficiency which allows calculation of the next stage inlet temperature and pressure by (Eq. (4)). Together with the given blade height they define the next stage inlet flow coefficient Φ corresponding to the given mass flow. This procedure is applied to all stages between inlet and exit and repeated for different mass flows between choking and minimum pressure drop. The resulting overall pressure ratio and efficiency of the 12 stage turbine are graphically presented in Fig. 17.

The power output at 318.5 kg/s is 546.8 MW with $\eta = 91$. This efficiency is the consequence of the very high stage loading and could be increased by lowering the loading per stage. This would require one or more additional stages at the same peripheral speed or to rotate faster with the same number of stages. The first option would make the turbine longer and could cause rotor-dynamics problems. The latter one would result in higher stresses.

7. Turbine blade cooling

Deformation and creep limit the maximum metal temperature of the turbine. A conjugate heat transfer analysis allows quantifying the hub cooling required to keep the blade root metal temperature below 1023 K. This is the maximum allowable temperature at the location of maximum stress to assure a 60 000 h lifetime for the turbine. Helium at 400 K is available at the compressor exit to cool the blade roots by impingement cooling or by cooling holes in the blade root. This very low temperature of the cooling fluid is a consequence of the inter-cooling between the LP and HP compressor and large specific heat of helium.

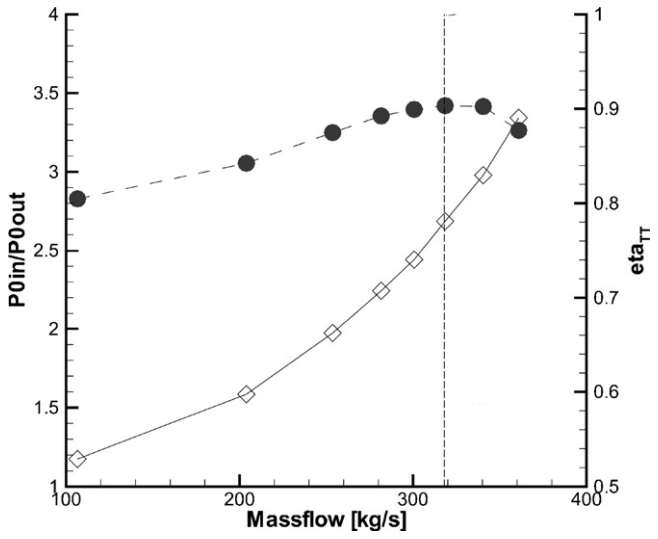

Fig. 17. The 12 stage turbine performance map.

The heat transfer calculations are made by coupling two codes: a non-adiabatic Navier–Stokes solver for the flow in the fluid domain and a Finite Element Analysis (FEA) for the heat conduction in the solid. Continuity of temperature and heat flux at the common boundaries is obtained by an iterative adjustment of the boundary conditions (Verstraete et al., 2007a,b). The advantage of the coupled approach is that one can use standard and well proven NS and FEA solvers and grid generators. Disadvantages of the coupled method are the need for an iterative procedure and the non-coinciding grids at the common boundary, requiring an interpolation to pass the boundary conditions from one grid to the other. The non-adiabatic flow is calculated by means of TRAFMS. The steady state heat transfer computation in the solid domain is predicted by the commercial FEA code SAMCEF using quadratic tetrahedral elements (Samcef FEA).

A first estimation of the blade wall temperature, together with the prescribed maximum temperature at the blade root provide all the boundary conditions needed for a FEA heat transfer calculation. The resulting metal temperature on the blade walls is then imposed as boundary conditions for a non-adiabatic Navier–Stokes calculation. The outcome of a new Navier–Stokes calculation is a more realistic heat flux on the blade walls to be used as boundary condition in the next FEA heat transfer calculation inside the blade. This procedure is repeated until convergence, i.e. until the wall temperature does not change anymore. The resulting temperature field on the blade wall is shown in Fig. 18. At the given turbine operating conditions, the total heat flux to be extracted is 300 W per blade root or a total of 41 kW for the first blade row.

Two geometries (cooling holes with 5 and 10 mm diameter and 50 mm length) have been analyzed with the available cooling gas flow conditions. The heat transfer in a pipe of diameter D and length L can be approximated by Dittus and Bölter (1930).

$$Q(m) = h\Delta T_{\ln}\frac{\pi D^2 L}{4} \tag{5}$$

where h is the heat transfer coefficient. Its value can be estimated from the Nusselt number, conductivity of the fluid ($k = 0.187$ W/(m K)) and hydraulic diameter D_H.

$$h = \frac{Nu\,k}{D_H} \tag{6}$$

$\Delta T_{\ln}$ is the logarithmic mean temperature difference, function of the cooling fluid inlet and outlet temperature and limit metal tem-

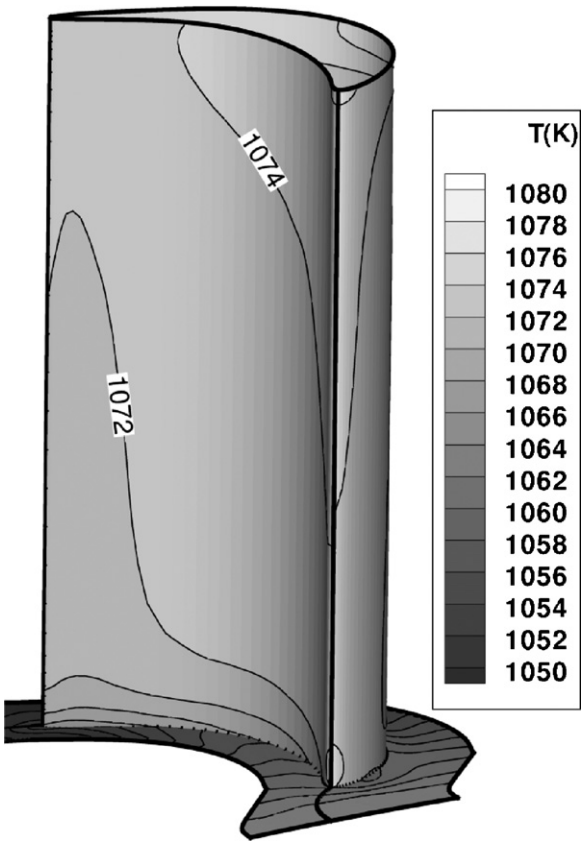

Fig. 18. Stator surface temperature for $T^{o}_{in} = 1202$ K and $T_{root} = 1023$ K.

perature ($T_s = 1023$ K) at the blade root.

$$\Delta T_{ln} = \frac{T_{out} - T_{in}}{\ln(T_s - T_{out}/T_s - T_{in})} \quad (7)$$

Simulations predict a total cooling mass flow in the 137 blades of:

27 g/s for one hole of 5 mm diameter per blade root.
54 g/s for one hole of 10 mm diameter per blade root.

The smaller cooling channel turns out to be more efficient because the higher fluid velocity compensates for the smaller cooling surface. The pressure drop is higher but negligible compared the 250 kPa that are needed to accelerate the fluid up to the rotor peripheral speed at the root section in order to assure a zero incidence at the cooling hole inlet. The first stator pressure drop is 395 kPa. Hence the stator outlet static pressure is sufficiently low to create this acceleration.

One can conclude from this that the amount of flow needed to cool the first rotor is negligible and will have only a marginal impact on the turbine performance. This very low cooling flow is a consequence of the low cooling fluid temperature, taken at the exit of the intercooled compressor, and the small difference between the main flow temperature and the maximum metal temperature.

8. Conclusions

The design of a multistage helium turbine for a direct cycle high temperature nuclear reactor gas turbine requires a multidisciplinary optimization to make a compromise between:

- the rotor peripheral speed, to limit the stresses;
- number of stages, to limit rotordynamic problems and cost and;
- maximum achievable efficiency.

The stepwise approach, described in this paper allows the design of a high performance turbine in agreement with the performance prediction correlations. It is shown that an extension to full 3D stator blades can be avoided.

The low Mach number flow facilitates the design of this multistage helium turbine. A typical performance map is presented and possible ways for further performance improvement are indicated.

An evaluation of the required cooling flow indicates that this has only a negligible impact on the cycle efficiency.

Acknowledgments

This project has been performed in the context of the 5th FP HTR-E project of the European commission under contract FIKI-CT-2001-00177. The authors also want to thank the other partners of this project for their stimulating discussions.

References

Arnone, A., 1994. Viscous analysis of three-dimensional rotor flow using a multigrid method. ASME Journal of Turbomachinery 116, 435–445.
Ballot, B., 2002. Present HTR Concepts and Large Associated Facilities. HTR/ECS 2002 High Temperature Reactor School, Cadarache, France.
Bammert, K., Krey, G., Küper, K.D., 1969. Performance of high-temperature reactors and helium turbines. Kerntechnik 11, 77–87.
Bammert, K., Deuster, G., 1974. Layout and present status of the closed-cyle turbine plant in Oberhausen. ASME Paper 74-GT-132.
De Michele, C., MacDonald, P., Sieverding, C., 1975. Meanline-Streamline Analysis Program. von Karman Institute PR, pp. 1975–2013.
Dittus, F.W., Bölter L.M., 1930. Heat transfer in automotive radiators of tubular type. University of California Publications on Engineering 2, p. 433.
Leonard, O, Van den Braembussche, R.A., 1992. Design method for subsonic and transonic cascades with prescribed Mach number distribution. ASME Journal of Turbomachinery 114, 553–560.
McDonald C.F., Adams R.G., Bell, F.R. Fortescue, P., 1975. Component design considerations for gas turbine HTGR power plant. ASME Paper 75-GT-67.
Muto, Y., Ishiyama, S., Tanuma, T., Kishibe, T., Matsumoto, I., 1999. Design Study of Helium Turbine for the 600 MWt HTGR-GT Power Plant. IGTC'99 Kobe TS-6, 3131-320.
Pierret, S., Van den Braembussche, R.A., 1999a. Turbomachinery blade design using a Navier–Stokes solver and Artificial Neural Network. ASME Journal of Turbomachinery 121–2, 326–332.
Pierret, S., Van den Braembussche, R.A., 1999b. Three-dimensional turbine blade design using a Navier–Stokes solver and Artificial Neural Network. In: Proceedings European Turbomachinery Conference, London, pp. 113–122 (IMechE C557/154/99).
Roberts, S.K., Sjolander, S.A., 2005. Effect of the specific heat ratio on the aerodynamic performance of turbomachinery. ASME Journal of Engineering for Gas Turbines and Power 127, 773–780.
Samcef FEA code by Samtech Group, www.samcef.com.
Sieverding, C.H., 1985a. Recent progress in the understanding of basic aspects of secondary flows in turbine blade passages. ASME Journal of Engineering for Gas Turbines and Power 107, 248–257.
Sieverding, C., 1985b. Axial turbine performance prediction methods in thermodynamics and fluid dynamics of turbomachinery. NATO ASI Series E, Applied Sciences (No. 97B), 737–784.
Smith, S.F., 1965. A simple correlation of turbine efficiency. Journal of Royal Aeronautical Society 69, 467.
Van den Braembussche, R.A., Leonard, O., Neckmouche, L., 1989. Subsonic and transonic blade design by means of analysis codes. AGARD Conference Proceedings 463, paper 9.
Verstraete, T., Alsalihi, Z., Van den Braembussche, R.A., 2007a. Numerical study of the heat transfer in micro gas turbines. ASME Journal of Turbomachinery 129–4, 645–856.
Verstraete, T., Alsalihi, Z., Van den Braembussche, R.A., 2007b. A comparison of heat transfer methods applied to an axial helium turbine. Proceedings of IMechE, J. Power and Energy 122-A, 981–989.
Yershov, S.V., Rusanov, A.V., Yakovlev, V.A., 2007. Optimisation of turbomachinery blade shapes using 3D viscous flow computations. In: Proceedings Seventh Turbomachinery Conference, Athens, Greece.